Cement & Concrete Composites 33 (2011) 906–917

Contents lists available at ScienceDirect

Cement & Concrete Composites

journal homepage: www.elsevier.com/locate/cemconcomp

Analysis of crack propagation due to rebar corrosion using RBSM

Khoa Kim Tran *, Hikaru Nakamura, Keisuke Kawamura, Minoru Kunieda

Department of Civil Engineering, Nagoya University, Chikusa-ku, Nagoya 464-8603, Japan

ARTICLE INFO

Article history:
Received 21 June 2010
Received in revised form 29 May 2011
Accepted 2 June 2011
Available online 16 June 2011

Keywords:
Rigid-Body-Spring Model
Corrosion–expansion model
Crack width
Internal crack
Electric corrosion test
Surface deformation

ABSTRACT

Cracking behavior due to rebar corrosion in concrete specimens having a single rebar is evaluated experimentally and analytically. In the experiments, in which corrosion was induced electronically, the propagation of cracks (including internal crack patterns and surface crack widths) was monitored. In addition, deformation of the specimen surface was measured using a laser displacement meter. In the analysis, a three-dimensional Rigid-Body-Spring Method (RBSM), combined with a three-phase material corrosion–expansion model, is proposed to simulate crack propagation due to rebar corrosion. The effects of the properties of corrosion products such as elastic modulus, penetration of corrosion products into cracks, and local corrosion after cracking of the concrete are investigated. Cracking behavior due to rebar corrosion is simulated reasonably well. The simulations using RBSM provide insight into the mechanisms of crack initiation and propagation due to rebar corrosion.

1. Introduction

Cracking of concrete due to rebar corrosion is a major source of deterioration of concrete structures. Such cracking typically accelerates the corrosion and deterioration processes, and can involve spalling of the concrete cover. It is necessary to assess internal damage from observable surface conditions during maintenance procedures. Therefore, it is desirable to establish a prediction method that can quantitatively evaluate internal crack propagation behavior and the rebar corrosion amount from observing surface cracks. Internal crack patterns due to rebar corrosion, considering differences of cover thickness or diameter of rebar, were clarified in past studies [1,2]. However, the relationships between propagating surface and internal cracks, as well as the dependence of surface crack opening on internal cracking, are still unclear. The basic effects of penetration of corrosion products into cracks after cracking of concrete on the internal expansion pressure are known and several simple models have been recommended [3,4]. However, assessment of these effects has not been done quantitatively. Moreover, the effect of local corrosion [5] and the local penetration of corrosion products into cracks after the initiation of cracking have not been reported in the literature.

In this study, crack propagation behavior due to rebar corrosion is investigated both analytically and experimentally. In the experiment, corrosion is induced by electrical means and the propagation of cracks is monitored. The surface crack widths are then measured and internal crack patterns are observed at several rebar corrosion amounts. In addition, deformation of the specimen surface is measured using a laser displacement meter to understand the relation between surface deformation and crack propagation. Crack propagation behavior is simulated using the Rigid-Body-Spring Method (RBSM) with three-dimensional Voronoi particles. In the analysis, a three-phase material model including concrete, steel reinforcement, and corrosion products layer is proposed. For the corrosion products layer, internal expansion pressure due to corrosion expansion is modeled as an initial strain problem and the stiffness of corrosion products is recommended. Moreover, the effects of penetration of corrosion products into cracks, local corrosion and local penetration of corrosion products into cracks during the corrosion process are simulated and the effects are quantitatively evaluated. The applicability of the model is verified by comparison with the experimental results. As a result, the effects of modeling and the mechanism of crack propagation such as crack initiation, progress of surface crack width, propagation behavior of internal cracks and the effect of internal cracks on surface crack width are clarified.

2. Experimental study

2.1. Electric corrosion test

Six single-rebar specimens with the dimensions shown in Fig. 1 were tested by means of an electric corrosion test. Table 1 shows the mixture proportions of the concrete used to cast the specimens. Before casting the concrete, the rebar of each specimen was weighed to obtain the initial weight. After casting the concrete, the specimens were cured in a room at 20 °C. After 32 days of

* Corresponding author. Tel.: +81 52 789 4484; fax: +81 52 789 1664.
E-mail addresses: tk.khoa@gmail.com (K.K. Tran), hikaru@civil.nagoya-u.ac.jp (H. Nakamura), kunieda@civil.nagoya-u.ac.jp (M. Kunieda).

0958-9465/$ - see front matter © 2011 Elsevier Ltd. All rights reserved.
doi:10.1016/j.cemconcomp.2011.06.001

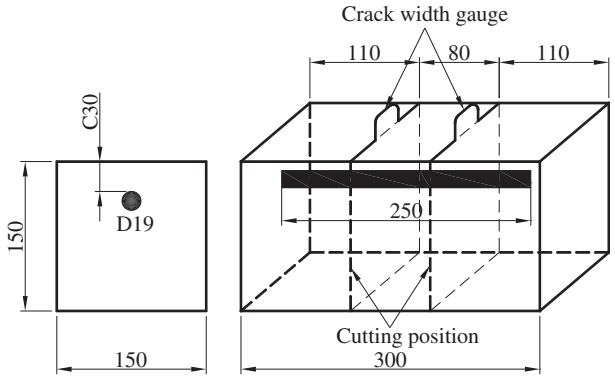

Fig. 1. Specimen dimensions.

Table 1
Mixture proportions of concrete.

W/C (%)	S/a (%)	Unit (kg/m^3)				
		Water	Cement	Sand	Aggregate	AE (liter/m^3)
56.5	44.0	166	294	779	990	1.18

W/C is the water/cement weight ratio.
S/a is the river sand/total aggregate volume ratio.
AE is a water reducing agent.

curing, the electric corrosion test was conducted. In order to accelerate the corrosion process, an external direct electric current of 900 μA/cm^2 was applied. A schematic of the electric corrosion test is shown in Fig. 2.

Prior to the test, the concrete compressive strength and tensile strength were determined to be 18.5 MPa and 1.53 MPa, respectively. During the test, surface crack widths were recorded using crack gauges and logged in computer files. The testing time was varied for the six specimens to investigate crack patterns and crack width propagation against the corrosion amount of the rebar. After each test was completed, the specimen was cut at the positions shown in Fig. 1 to enable observation of the internal crack patterns and measurement of the internal crack widths and lengths. The rebar was cleaned using a steel brush and corrosion products were removed from the sound steel by immersing the rebar in a 10% ammonium citrate solution for 24 h. The difference between the initial weight and the remaining weight after the corrosion test is the mass loss W (g) of the rebar in each specimen. Fig. 3 shows a relation between mass loss W and testing time t. Based on the experimental data, an empirical equation to calculate rebar mass loss was derived as follows [6,7]:

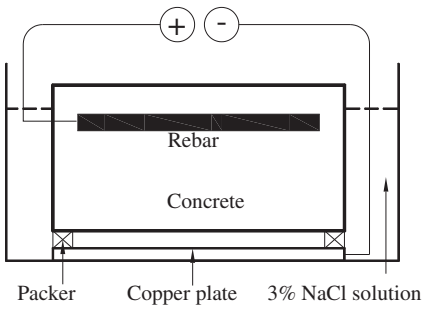

Fig. 2. Schematic of corrosion test.

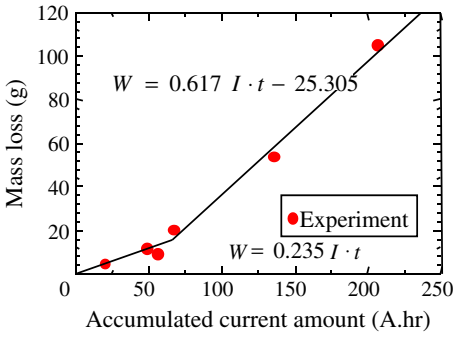

Fig. 3. Mass loss computation.

$$\begin{aligned} W &= 0.235 I.t \qquad (I \cdot t < 66\ \mathrm{A \cdot h}) \\ W &= 0.617 I \cdot t - 25.305 \quad (I \cdot t > 66\ \mathrm{A \cdot h}) \end{aligned} \tag{1}$$

where W, I and t are rebar mass loss (g), current intensity (A) and testing time (h) respectively.

Corrosion amount of the rebar W_r (mg/cm^2) during the testing is determined by dividing the mass loss W (mg) by the wet surface of the rebar (cm^2).

$$W_r = \frac{W}{\pi D \cdot L} \tag{2}$$

where D and L are initial rebar diameter (cm) and rebar length (cm), respectively.

2.2. Surface crack propagation

Based on the empirical Eq. (1) and the logged data of surface crack widths, the propagation of surface crack width against corrosion amount was developed, as shown in Fig. 4. The opening of a surface crack initiates after a significant amount of corrosion products is formed. A critical amount of corrosion products is required to build up enough expansion stress and to cause cracking in the surface of a concrete specimen as Oh et al. discussed [8]. After the crack initiation, the surface crack width rapidly propagates up to a value of about 0.4 mm. After that, the speed of propagation slows with the occurrence of lateral cracks and the effect of the penetration of corrosion products into cracks, which is discussed later in this study. Then, the speed of propagation increases once again.

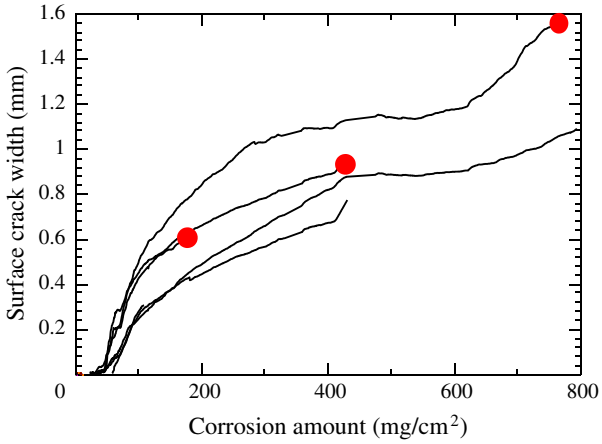

Fig. 4. Surface crack propagation.

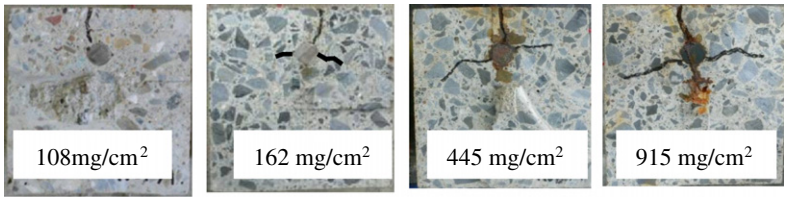

Fig. 5. Internal crack patterns at several corrosion amounts.

2.3. Crack pattern

Internal crack patterns of specimens at several corrosion amounts, corresponding to the dots plotted in Fig. 4 are shown in Fig. 5. The initiation of a visible crack occurs on the surface of the concrete (vertical crack). When the amount of corrosion products increases, the crack propagates to the rebar. After that, lateral cracks appear and their lengths increase along with the increase in surface crack width.

2.4. Surface deformation

When rebar corrodes, the concrete cover is deformed due to internal expansion pressure and the tensile stress reaches maximum on the cover surface just above the rebar [9]. When the tensile stress exceeds the concrete tensile strength, a minor crack will occur and this will develop to become a visible one. In order to understand the relation between crack propagation and deformation of the specimen surface due to rebar corrosion, the vertical deformation of specimen surface is measured during the corrosion process using a laser displacement meter having an accuracy of 1 μm (Fig. 6).

Due to the weight limitation of the laser equipment, a new set of specimens with a length of 200 mm was prepared. The other dimensions of the specimens and the concrete mixture composition were the same as shown in Fig. 1 and Table 1. At the start of the electric corrosion test, the concrete compressive strength was 19.8 MPa.

Vertical deformation was measured at points 75 mm and 125 mm from the end of each specimen (the red dashed lines in Fig. 7[1]). For each measuring line, the starting point is 10 mm in from the specimen edges and the measurement is 130 mm. The measurement interval was 250 μm (0.25 mm).

Surface vertical deformation was measured at several surface crack width values monitored by the data logger during the electric corrosion process. A Fast Fourier Transform was conducted to remove the effects of imperceptible vibrations of the specimens and then an Inverse Fourier Transform was conducted to obtain surface deformation. Microwaves with frequencies of more than five wave periods in each 10 mm of length were eliminated in the process [10].

Each specimen was measured at the beginning of the corrosion test (day 0) to obtain the initial surface levels. The difference between the initial surface level and the measurement level at each measurement time is the deformation of the specimen surface at the measuring time.

Fig. 7 shows the measurement surface deformation of specimens Nos. 1 and 2 at minor surface crack widths (Fig. 7a) and visible surface crack widths (Fig. 7b). After measuring deformation at visible crack widths, the specimens were cut to enable observation of corresponding internal crack patterns (Fig. 7c).

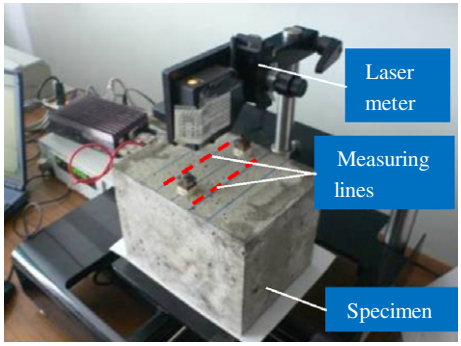

Fig. 6. Laser displacement meter to measure surface deformation.

The deformation of the specimen surfaces is small (approximately 25 μm), corresponding to minor surface crack widths (0.012 mm or 0.054 mm) in which a visible crack is not observed. With the addition of more corrosion products, the deformation of the surface specimens increases and surface crack width increases accordingly (Fig. 7b). It is interesting that surface deformation reaches a maximum value where the surface crack initiates. When lateral cracks initiate and propagate, the distribution of the surface deformation is closely related to the lateral crack patterns; see the dashed lines between Fig. 7b and c. For example, when internal cracks propagate diagonally (right side crack in Fig. 7c of specimen No. 2), surface deformation is not increased.

3. Analytical model

3.1. Three-dimensional RBSM

The RBSM developed by Kawai and Takeuchi employs a discrete numerical analysis method [11,12]. Analyses of concrete or concrete structures using the RBSM have been conducted by Bolander and Saito [13], Ueda et al. [14] and Nagai et al. [15].

The RBSM represents a continuum material as an assemblage of rigid particle elements interconnected by zero-length springs along their boundaries as shown in Fig. 8. In this study, three-dimensional RBSM is used [16]. Each element has six degrees of freedom at the center points. The boundary between two elements is divided into triangles formed by the center and vertices of the boundary. At each center point of a triangle, three springs- one normal and two shear springs- are set. The analytical model is divided into elements using Voronoi random polygons. In a RBSM model, crack widths can be automatically measured during analysis so it is convenient to directly calculate the volume of cracks in the analysis. It is possible to simulate complicated problems using the three-dimensional RBSM model.

[1] For interpretation of color in Figs. 7 and 30, the reader is referred to the web version of this article.

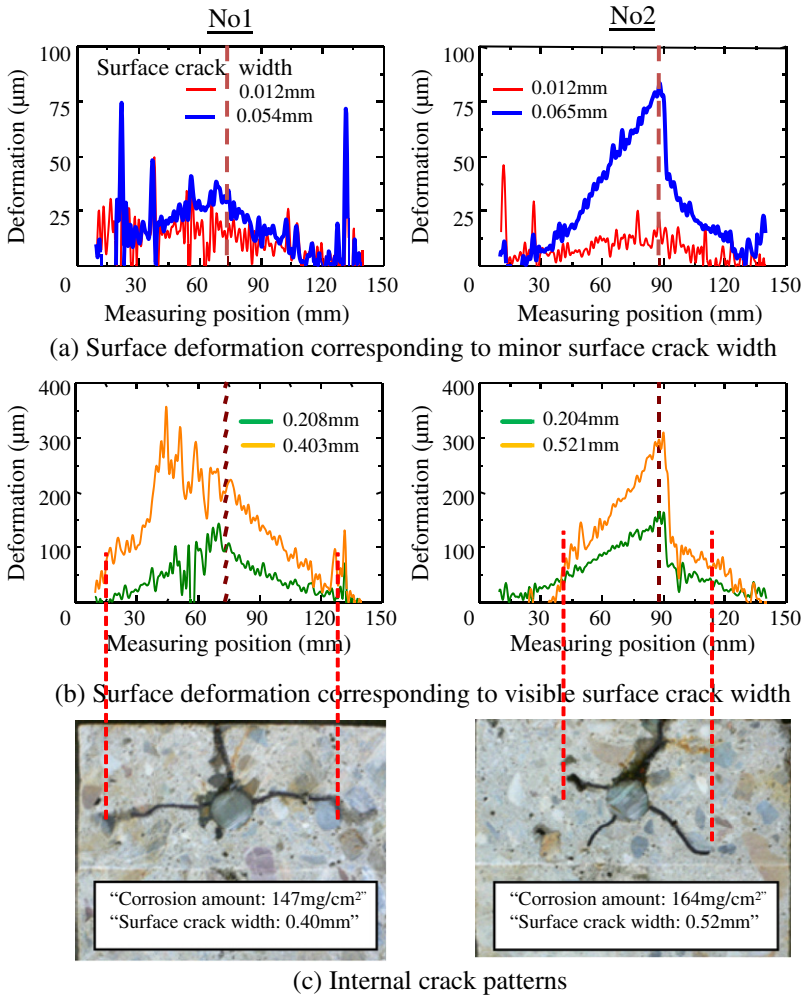

Fig. 7. Measuring surface deformation.

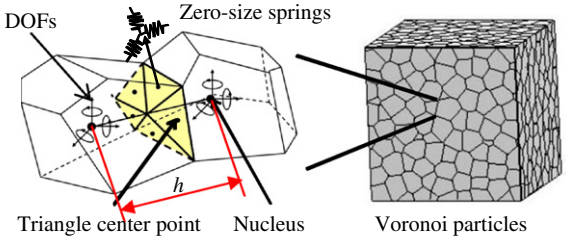

Fig. 8. Voronoi particle definition of RSBM element.

In the analysis, a stiffness matrix is constructed based on the principle of virtual work [12], and the modified Newton–Raphson method is employed for the convergence algorithm. In the convergence process, displacements that cancel the unbalanced force of elements are added to the elements. The displacements are calculated using the stiffness matrix. Convergence of the model is judged when the ratio of Σ(Unbalanced force of element in the model)^2 to Σ(Applied force to element)^2 becomes less than 10^{-6}. When the model does not converge at a given maximum iterative calculation number, the analysis proceeds to the next step [15].

3.2. Concrete material model

Fig. 9 shows the concrete material models that are used in the analysis.

The tensile behavior of concrete up to the tensile strength is modeled as linear elastic. A bilinear softening branch is assumed after cracking as shown, in which f_t is tensile strength, G_F is tensile fracture energy (=0.0525 N/mm in this study) and h is distance between centers of the Voronoi elements.

In the compressive model, the stress–strain relationship is parabolic up to the compressive strength f'_c. The initial stiffness, E, is Young's modulus of concrete, E = 21.7 GPa in this study.

Normal springs are set to represent the tensile and compressive properties of concrete. Strain of the normal springs is defined as follows:

$$\varepsilon = \frac{\Delta n}{h} \tag{3}$$

where ε is strain of the normal springs and Δn is normal relative displacement of elements of those springs [15].

Tangential (shear) springs represent the shear transferring-mechanism of concrete. Strain of the shear springs is defined as follows:

$$\gamma = \frac{\Delta s}{h} \tag{4}$$

where γ is strain of the shear springs and Δs is shear relative displacement of elements of those springs [15].

The shear strength is assumed to follow the Mohr–Coulomb type criterion with the tension and compression caps, in which, c

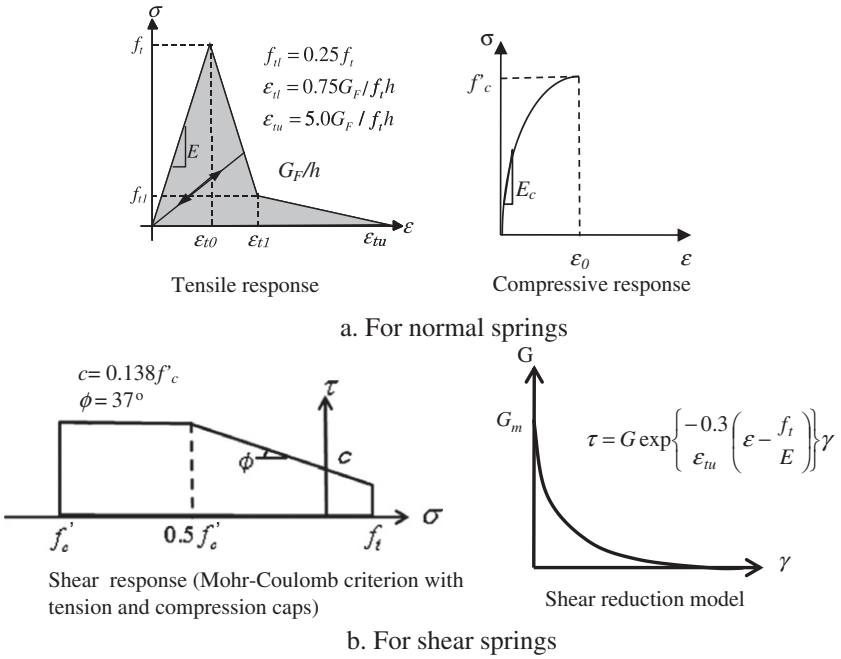

Fig. 9. Concrete material model.

is cohesion and ϕ is internal friction and τ is shear stress. The shear–fracture criterion is expressed as follows [17]:

$$\frac{\tau^2}{\tau_f^2} \geqslant 1 \tag{5}$$

where

$$\tau_f = \begin{cases} c - \sigma \tan\phi, & \text{for} \quad \sigma \geqslant 0.5 f'_c \\ c - 0.5 f'_c \tan\phi, & \text{for} \quad \sigma < 0.5 f'_c \end{cases} \tag{6}$$

After the shear stress reaches the yield strength, the stress moves on the yield surface until the shear strain reaches the ultimate strain γ_u. The force in the shear spring is released and the local stiffness is set to zero when the shear strain exceeds the ultimate strain. The ultimate strain is set to 4000 μ in this study.

The shear transferring capacity at the cracked interface changes according to the crack opening. In order to take account of this effect, the shear stiffness is reduced by using a function of the strain normal to the crack as shown in the shear-reduction model in Fig. 9b, in which G is the shear stiffness.

Springs set on boundary behave elastically until stresses reach the τ_{max} criterion or the tensile strength f_t [15].

Rebar is modeled as linear elastic in the analysis with the modulus of elasticity being 200 GPa.

3.3. Corrosion expansion model

In the RBSM model, the expansion of corrosion products is modeled as shown in Fig. 10. A three-phase material model including rebar, corrosion products and concrete is applied. The merit of the model is that the properties of corrosion products such as thickness (H) and elastic modulus (E_r) are directly assumed. The model is also efficient in investigating the effects of corrosion products.

The thickness of corrosion products layer (H) is kept constant during the analysis. This is a fictitious thickness used in the simulation in this study.

The corrosion products layer is modeled by an elastic material model with unloading occurs to the origin. Due to nature of the corrosion process, we assume that internal expansion pressure is only activated in the normal direction, so strain is applied only to the normal springs located on the boundary between the corrosion products layer and the rebar. Strain in the corrosion product layer is determined [18]:

$$\varepsilon_{cor} = \frac{U_{cor} - U}{H} \tag{7}$$

where U_{cor} is the real increase of the rebar radius corresponding to confinement of the concrete and U is the free increase of the rebar radius. On the other hand, shear stiffness of shears springs of the corrosion products layer is set nearly zero in the analysis to simulate free sliding of corrosion products layer in the shear direction.

Normal stress distribution in the corrosion products layer is determined based on the linear stress–strain relationship. Increment of a normal stress in the corrosion layer at each analysis step is determined as follows:

$$\Delta\sigma_{cor} = E_r(\Delta\varepsilon - \Delta\varepsilon_0) \tag{8}$$

in which, $\varepsilon = \frac{U_{cor}}{H}$ is total strain and $\varepsilon_0 = \frac{U}{H}$ is initial strain.

The internal expansion due to rebar corrosion is simulated using the initial strain problem with increment of initial strain in each analysis step is determined as Eq. (9) and it is an input data in the analysis.

$$\Delta\varepsilon_0 = \frac{\Delta U}{H} \tag{9}$$

in which, ΔU is an increment of the free increase U in each analysis step.

U is computed from the corrosion amount (W_r) as follows [19]:

Based on Fig. 11, the volume of steel loss is:

$$V_{\text{loss}} = L[\pi r^2 - \pi(r-x)^2] = \pi L[2r \cdot x - x^2] \approx 2\pi \cdot L \cdot r \cdot x, \quad \text{since } x^2 \approx 0 \tag{10}$$

Volume of corrosion products:

$$V_{cor} = L[\pi(r+U)^2 - \pi(r-x)^2] \approx 2\pi L \cdot r(U+x) \quad \text{since } x^2 \approx 0 \quad \text{and} \quad U^2 \approx 0 \tag{11}$$

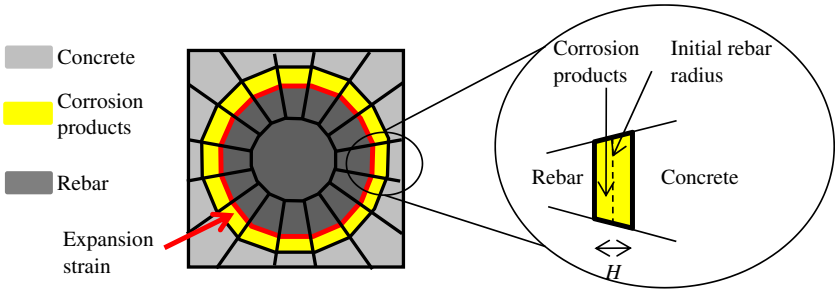

Fig. 10. RBSM corrosion expansion model.

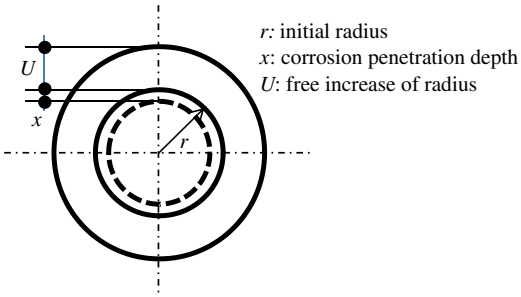

Fig. 11. Physical dimensions of corrosion model.

α_{cor} is the volume-expansion ratio of corrosion products, which depends on the corrosion products that are formed [18], in this study, it is assumed as 2.5 [19]. As definition of α_{cor}:

$$\alpha_{cor} \cdot V_{loss} = V_{cor} \tag{12}$$

So,

$$\alpha_{cor} \cdot 2\pi L \cdot r \cdot x = 2\pi L \cdot r(U + x) \tag{13}$$

Or

$$x = \frac{U}{\alpha_{cor} - 1} \tag{14}$$

W_r is defined as shown in Eq. (2) and with Eqs. (10) and (14):

$$W_r = \frac{\rho_s \cdot V_{loss}}{2\pi r \cdot L} = \rho_s \cdot x = \frac{\rho_s \cdot U}{\alpha_{cor} - 1}, \quad \text{or,} \quad U = \frac{W_r \cdot (\alpha_{cor} - 1)}{\rho_s} \tag{15}$$

in which, ρ_s is rebar density (7.85×10^3 mg/cm^3).

3.4. Modeling of local corrosion

The chloride diffusivity coefficient through cracked concrete is much more than through sound concrete [5]. As a result, a rebar is much more corroded around a part surrounded by uncracked concrete or concrete with only minor cracks.

Fig. 12 shows the experimental results of local corrosion of rebar corresponding to the internal crack patterns. Local corrosion can be observed near the vertical crack.

In this study, local corrosion of rebar after crack initiation is simply assumed as follows:

- Rebar is locally corroded when a vertical crack near the rebar exceeds 0.1 mm in width.
- The local corrosion model is a QUARTER corrosion model or a HALF corrosion model as shown in Fig. 13.
- At the same corrosion amount, the total amount of corrosion products in the local corrosion model (S_L) is the same as that in the uniform model (S_u).

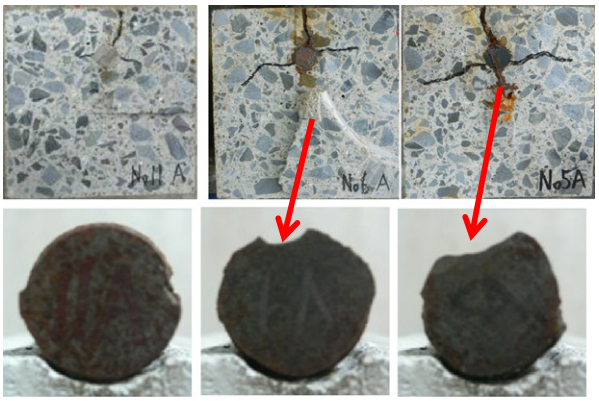

Fig. 12. Locally corroded rebar.

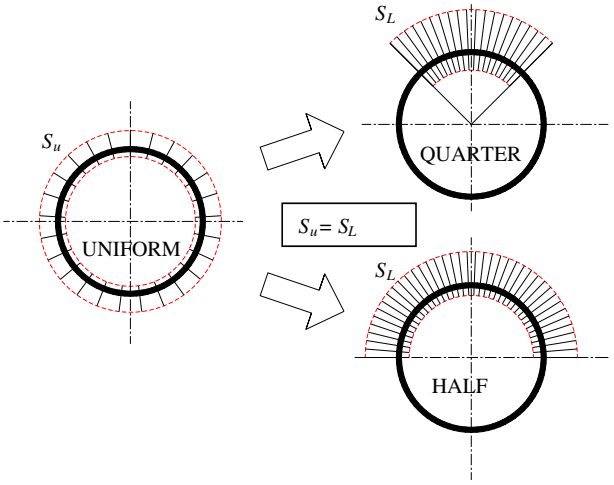

Fig. 13. Local corrosion models.

- Increment of initial strain in Eq. (9) is only applied over HALF or one-QUARTER of the model.

3.5. Modeling of local penetration of corrosion products into cracks

During the corrosion process, it has been shown that corrosion products will penetrate into cracks after the concrete cracks and this effect may reduce the internal expansion pressure on concrete due to rebar corrosion [3,4].

From the experiments, the penetration of corrosion products into cracks could be observed and most of the corrosion products penetrated into vertical cracks in the concrete cover thickness as shown in Fig. 14. The penetration can be diagrammatically modeled as in Fig. 15.

This effect is simulated in the RBSM analysis. One of the advantages of the RBSM model is that crack widths and volume of the cracks can be calculated directly during the analysis. It is therefore convenient to calculate the reduction in volume of corrosion products that penetrate into cracks. The reduction in the internal expansion pressure caused by the penetration of corrosion products into cracks is calculated by reducing free increase U.

We have assumed the following when considering this effect in the analysis:

- Corrosion products can only penetrate into cracks if crack widths exceed the threshold value set for crack width. In this study, the threshold is assumed as 0.1 mm.
- Corrosion products fill the cracks fully.
- The free increase U is uniformly reduced around the rebar and then the HALF corrosion model in Section 3.4 is applied to redistribute the internal corrosion expansion pressure.

With a free increase of U, the corresponding corrosion product volume corresponding with the U value is (Fig. 11):

$$V_{cor,U} = [\pi(r+U)^2 - \pi r^2]L = \pi U(2r+U)L \tag{16}$$

as $U^2 \approx 0$, Eq. (16) can be approximated as

$$V_{cor,U} = 2\pi r \cdot U \cdot L \tag{17}$$

When the penetration of corrosion products into cracks is considered, the effective corrosion products volume $V_{cor,eff,U}$ is:

$$V_{cor,eff,U} = V_{cor,U} - V_{crk} \tag{18}$$

where V_{crk} is volume cracks computed in Fig. 16 in which only the volume of vertical cracks is taken into account based on the observation of the test results.

If the effective free increase is U_{eff}, U_{eff} can be determined from V_{crk} based on Eqs. (17) and (18) as follows:

$$U_{eff} = U - \frac{V_{crk}}{2\pi rL} \tag{19}$$

or, in terms of increment value at an analysis step:

$$\Delta U_{eff} = \Delta U - \frac{\Delta V_{crk}}{2\pi \cdot r \cdot L} \tag{20}$$

in which, ΔU_{eff} is effective increment of the free increase and ΔV_{crk} is increment of volume of cracks computed in Fig. 16.

The effect of the penetration of corrosion products into cracks is accounted for during the analysis. Increment of initial strain in Eq. (9) at an analytical step is reduced by ΔU_{eff} in Eq. (20)

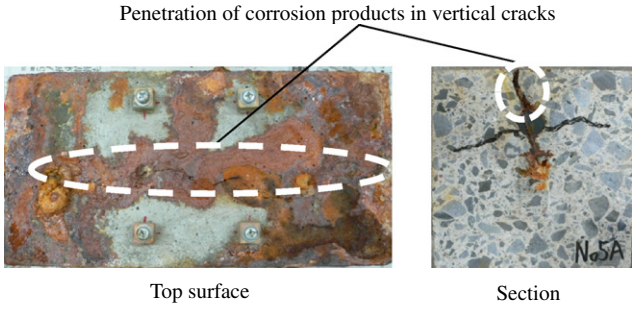

Fig. 14. Penetration of corrosion products into cracks.

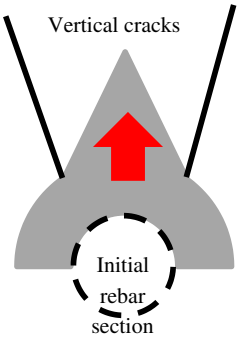

Fig. 15. Local penetration of corrosion products into cracks.

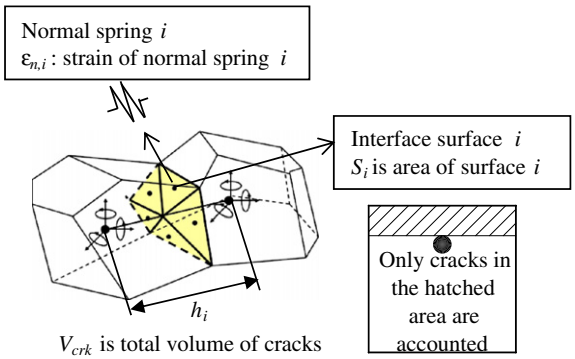

Fig. 16. Computation of crack volume to simulate local penetration of corrosion products into crack.

4. Analytical results

In the analysis, the mesh sizes of the Voronoi particles are 5 mm in the cover area and 10 mm in the other areas as shown in Fig. 17. Another arrangement of the Voronoi particles was tried to confirm the similarity of the analytical results.

It was not easy to measure the properties, such as thickness and linear elastic modulus, of the corrosion products in the experiments. We analyzed specimens with various values for the thickness and the linear elastic modulus of the corrosion products layer. As a result, in the RBSM model, a thickness (H) of 1.0 mm which is kept constant in the analysis as explained in Section 3.3

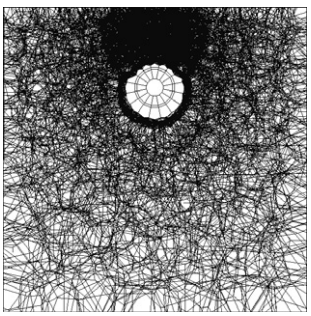

Fig. 17. RBSM model of specimen.

and an elastic modulus (E_r) of 500 MPa simulate reasonable cracking behavior in terms of crack patterns and surface crack width propagation in comparison with the experimental results. The local penetration combined with the local corrosion HALF model was applied to analyze the specimen.

4.1. Crack patterns

The deformation of a specimen at a corrosion amount of 300 mg/cm^2 is shown in Fig. 18. The cracking behavior, which is the same as the experimental results, demonstrates the merit of the RBSM model. Internal crack patterns at several surface crack widths are shown in Fig. 19. For clarity, only cracks wider than w_1, corresponding to ε_{tu} in Fig. 9a (where stress transfer is lost), as shown in the indication of crack width value in Fig. 19, are shown. The crack patterns are similar to the test results in Fig. 5, in which a visible crack initiates from the surface and propagates to the rebar. With a further amount of corrosion products, lateral cracks initiate and propagate.

4.2. Surface crack propagation

The analytical surface crack width propagation is compared with the experimental results as shown in Fig. 20. The analytical results agree with the experimental results, not only in terms of crack width values, but also propagation tendency. That is, the surface crack width initiates at a corrosion amount of around 40 mg/cm^2 of rebar and it propagates rapidly to a value of around 0.4 mm, then the crack width continues to increase but the speed of propagation reduces.

4.3. Internal crack propagation

It is necessary to simulate internal crack propagation to predict internal cracking behavior from surface cracks. The analytical results of propagations of near rebar cracks and lateral cracks are compared with the experimental results.

4.3.1. Propagations of near rebar vertical cracks

Fig. 21 shows the propagation of near rebar vertical cracks. As shown in the figure, after initiation, the near rebar crack width also increases when the corrosion amount increases. However, the propagation slope is much smaller than the one for surface crack width. The analytical result appears close to the experimental results.

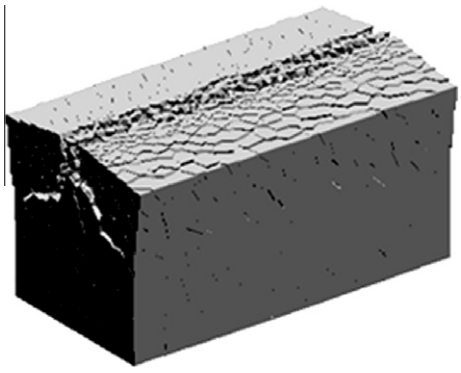

Fig. 18. Deformation due to rebar corrosion (magnification × 25) Corrosion amount: 300 mg/cm^2.

4.3.2. Propagations of lateral cracks

Fig. 22 shows the propagation of lateral crack length. Lateral crack length is measured from the side of the rebar to the tip of a visible lateral wider than w_1 as shown in the indication of crack width value (Fig. 19). The lateral crack length increases rapidly to a value of 40 mm after initiation which is at a corrosion amount around 100 mg/cm^2 corresponding to surface crack width value of about 0.4 mm. The crack length seems not to increase although the corrosion amount increases. The analytical results simulate well behavior such as, rapid increase in lateral crack length before a corrosion amount of 400 mg/cm^2 and the convergence behavior of the length in large amount of corrosion.

Fig. 23 shows the propagation of lateral crack width at several positions from a rebar (i.e. 10 mm and 40 mm). At 10 mm from the rebar, the lateral crack width gradually increases to a value around 0.6 mm after initiation but at 40 mm, the propagation of the lateral crack width slows to a value around 0.2 mm. This behavior appears to be simultaneous to the propagation of lateral crack length in Fig. 22. The analysis reasonably simulates crack width propagation as well as crack length.

4.4. Surface deformation

The proposed analytical model was applied to the specimen described in Section 2.4 and the analytical surface deformation was compared with the experimental results in Fig. 24. Deformation values are obtained corresponding to minor and visible surface crack widths. The analytical values agree reasonably well with the test values such as deformation area, deformation shape and deformation value.

Fig. 25 shows the propagation of vertical surface deformation at the cracking position (i.e. 75 mm from the specimen edge) against surface crack width (analytical results against experimental results). The propagation appears in a linear relationship and the analytical results agree with the experimental results.

5. Effects of modeling

The analytical model was applied with some changes in order to evaluate the effects of the corrosion products elastic modulus, corrosion expansion pressure distribution and penetration of corrosion products into cracks.

5.1. Effect of stiffness of corrosion products

The analytical mode was reapplied with a new value for the corrosion products elastic modulus E_r = 100 MPa. The analytical surface crack width propagation is compared with the one for E_r = 500 MPa presented in Section 4.2. At the same corrosion amount, with a higher value for the elastic modulus of, E_r = 500 MPa, the corrosion expansion pressure induced by corrosion products is larger than the one in the case of E_r = 100 MPa. In Fig. 26, the propagation in the case of E_r = 100 MPa is similar to the one of E_r = 500 MPa but the initiation of crack occurs at a higher corrosion amount value of about 100 mg/cm^2. In comparison with the experimental results, the value of the elastic modulus is important in evaluating crack initiation.

5.2. Effect of local corrosion

The local corrosion QUARTER model and the uniform corrosion model are applied and compared with the local HALF model as presented in Section 4.

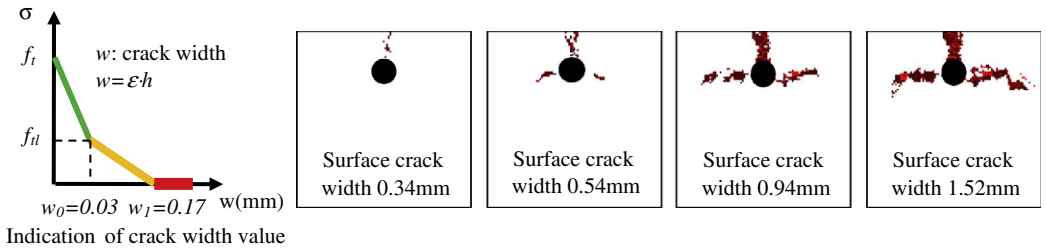

Fig. 19. Internal crack patterns.

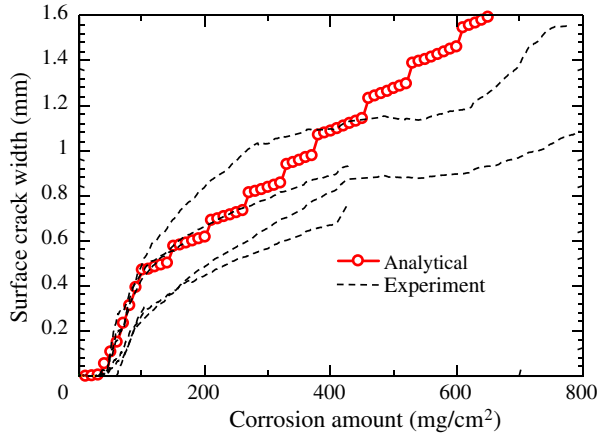

Fig. 20. Surface crack propagation.

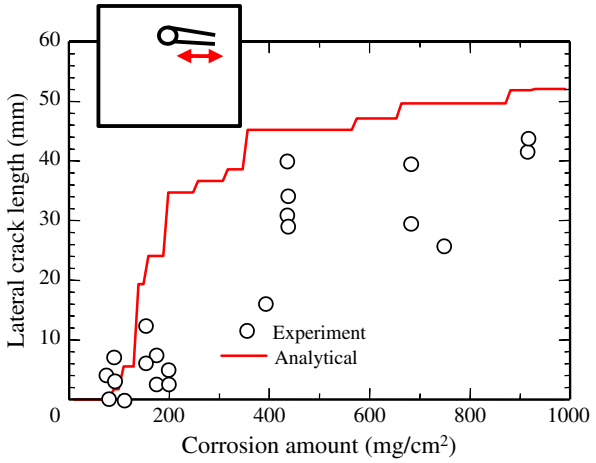

Fig. 22. Propagation of lateral cracks.

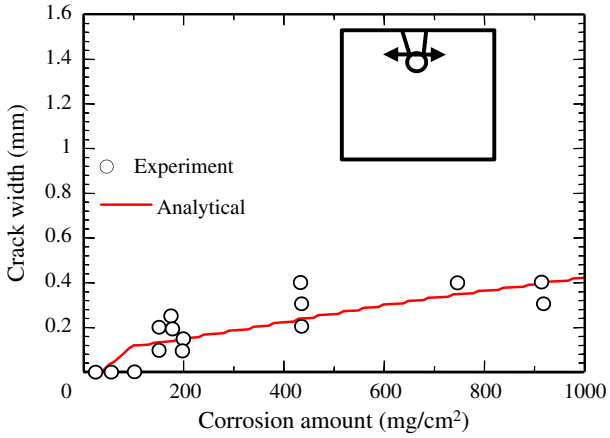

Fig. 21. Propagation of near rebar vertical cracks.

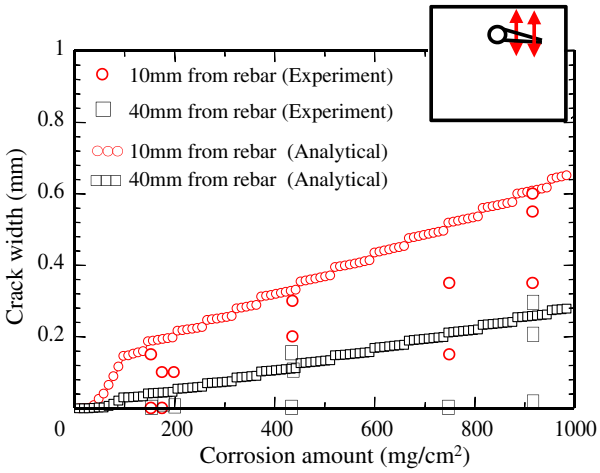

Fig. 23. Propagation of lateral crack width.

The surface crack opening propagation shows similar behavior for each model, such as the local corrosion (HALF or QUARTER) and the uniform model.

In terms of internal crack patterns, the behaviors of the local corrosion (HALF or QUARTER) and the uniform model are different as shown in Fig. 27. That is, at large amounts of corrosion, there are inside cracks propagating from the rebar conforming to the behavior of uniform corrosion. When uniform corrosion is assumed, corrosion expansion pressure acts in all direction around rebar. Then, the expansion pressure under the rebar causes an inside crack. The situation is different from the experiments for local corrosion. On the other hand, the crack patterns of the HALF model and the QUARTER model are the same. Therefore, the locally corroded area type (HALF or QUARTER) is not very sensitive in the analysis. The local corrosion model can better simulate crack patterns in comparison with the experimental results.

5.3. Effect of penetration of corrosion products into cracks

In order to evaluate the effect of penetration of corrosion products into cracks, an analysis was made again without the penetration effect and with the penetration effect but the threshold value for the crack width given in Section 3.5 was changed to 0.2 mm.

Fig. 28 shows analytical surface crack width propagations in comparison with the experimental results. Without the penetration effect, the internal expansion pressure is highest and it causes

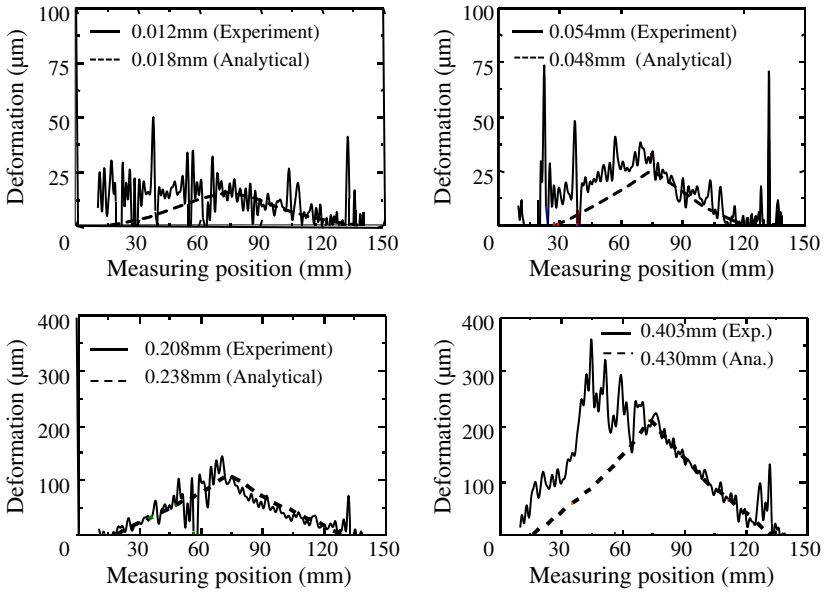

Fig. 24. Analytical deformation corresponding to surface crack widths.

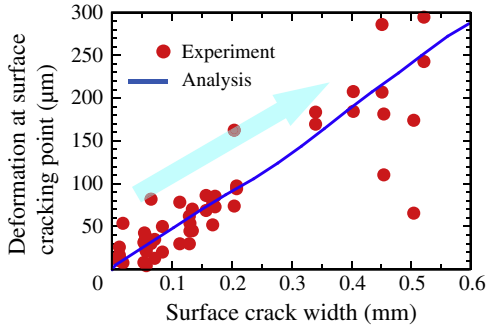

Fig. 25. Deformation value at cracking point against surface crack width.

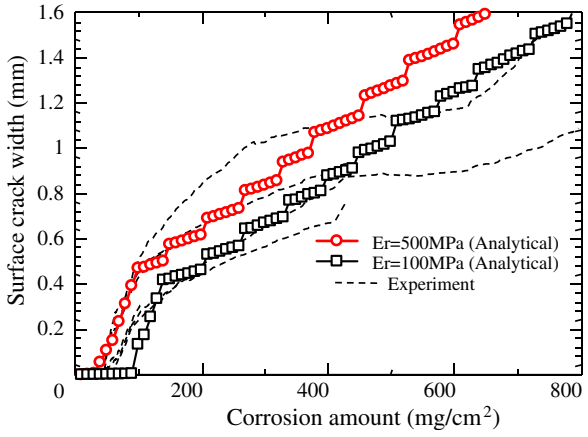

Fig. 26. Dependence of surface crack width on *Er* value.

the biggest crack width at the same corrosion amount value. Also, the surface crack width proportionally increases with the corrosion amount. In this case, the crack width values appear to be overestimated against the experimental results especially in the later stage of the corrosion process.

When penetration is taken into account, and with an assumed crack width threshold of 0.1 mm, the propagation speed of the

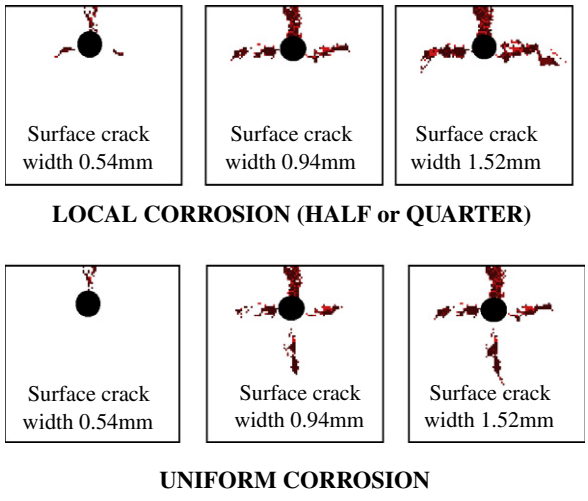

Fig. 27. Internal crack patterns (Local corrosion and uniform corrosion).

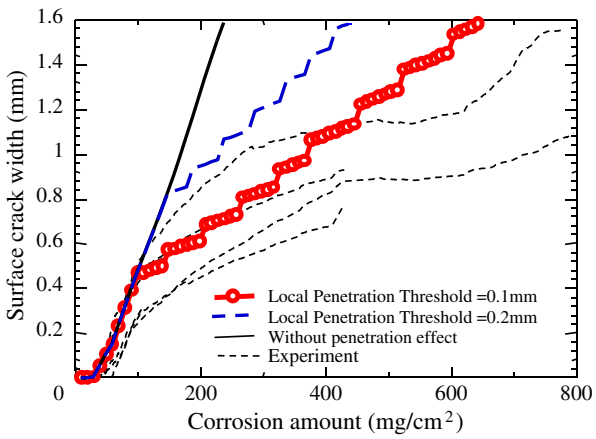

Fig. 28. Surface crack propagation.

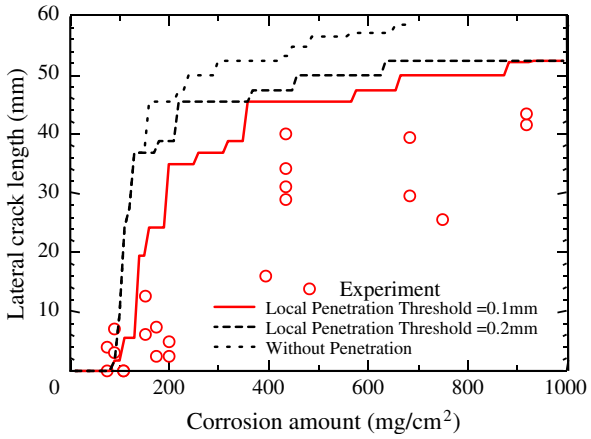

Fig. 29. Propagation of lateral crack length.

surface crack width is reduced at the point corresponding to a surface crack width value of about 0.40 mm. At this point, the internal crack is bigger than the threshold value, so corrosion products penetrate into the cracks and induce a reduction in the internal corrosion expansion pressure. Therefore, the penetration behavior is important to accurately simulate an evaluation of cracking with propagation. With threshold of 0.2 mm, the changing point of propagation corresponds to a crack width of 0.8 mm because there is small amount of fewer corrosion products penetrating into the cracks in this case. The tendency of crack width propagation after the changing point is similar to the case of a threshold of 0.1 mm. Fig. 29 shows the propagation of lateral crack length without penetration effect, and with a penetration effect with thresholds of 0.1 mm and 0.2 mm. In the case of penetration with different threshold values, the propagation in the early stage after cracking is clearly different but in the later stage with very large amounts of corrosion, the lateral crack length appears to convergence to a value of about 50 mm for both threshold values. Therefore, the penetration of corrosion products into cracks not only affects the surface crack width propagation, but also internal crack propagation.

As shown in Fig. 28, a corrosion model that takes into consideration the penetration effect at a threshold of 0.1 mm simulates crack width propagation most closely to the experimental results. The threshold value greatly affects surface crack width propagation. In the experiments, corrosion products may not fully penetrate into cracks and the speed of penetration depends on crack width and the properties of corrosion products. In the analysis, we have assumed the fastest and most penetration, which induces the largest reduction in corrosion expansion. The above assumptions are simple cases for the analysis in this study and it will definitely require further work to simulate this effect. More experiments are needed to validate the simulations.

6. Crack propagation mechanism

6.1. Crack initiation

Fig. 30 shows the initiation of minor cracks and visible cracks based on the analytical results. Fig. 30a shows crack width values corresponding to the colors (green, yellow and red) shown in analytical crack patterns. States with green and yellow lines correspond to minor cracks and the state with a red line, in which stress transfer is lost, corresponds to a visible crack. Fig. 30b shows areas of minor cracks and visible cracks with the surface crack width propagation. Based on the analytical crack pattern and surface deformation (Fig. 30c), minor cracks initiate around rebar when the tensile stress just exceeds the concrete tensile strength (f_t) (green crack pattern). With a further amount of corrosion products forming on rebar, minor cracks propagate from the rebar and surface deformation occurs due to expansion pressure. Then, a minor crack initiates from the surface and surface deformation is further increased and minor cracks are accumulated in the con-

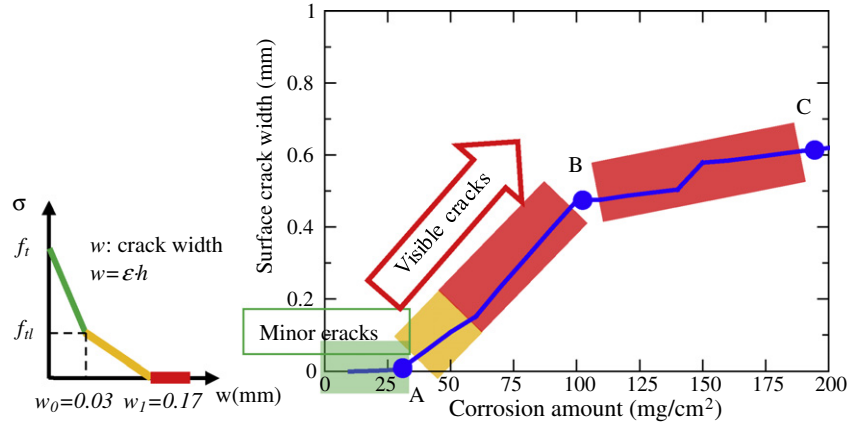

(a) Indication of crack width value **(b)** Analytical surface crack width propagation

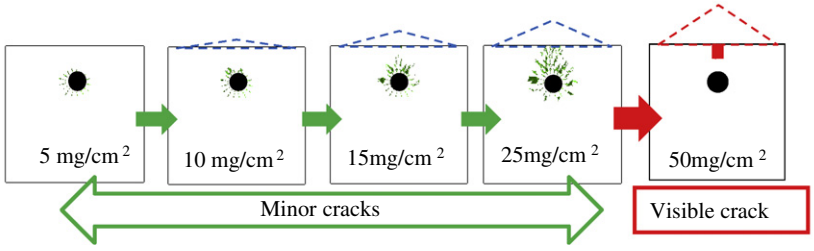

(c) Crack pattern development with surface deformation

Fig. 30. Initiation of minor cracks and visible crack (analytical).

crete cover thickness from both sides, i.e. rebar and surface. When the corrosion amount increases to a given value, cracks becomes visible on the surface (red crack pattern) corresponding to the bending effect of the surface due to the internal expansion pressure. This behavior is confirmed by measuring surface deformation using the laser displacement meter shown in Fig. 7.

6.2. Crack propagation (visible cracks)

From the surface crack width propagation (Fig. 30b) and the internal crack propagations (Figs. 21–23), a mechanism of surface visible crack width propagation with internal crack propagation can be proposed as follows:

(a) When rebar corrodes, minor cracks are formed around the rebar when the tensile stress in concrete exceeds the concrete tensile strength. With an increase in the amount of corrosion products, a visible crack is initiated from the concrete surface due to the bending of the surface and it propagates to the rebar. In this stage, the surface crack width rapidly increases corresponding to stages A and B in Fig. 30b due to stress release for the brittle behavior after cracking.
(b) Then, lateral cracks initiate and then increase in their widths and lengths simultaneously. Corrosion products penetrate into internal cracks at this stage and reduce the speed of surface crack width propagation in comparison with the previous stages (stages B and C in Fig. 30b).

7. Conclusion

The purpose of this study has been to propose an analytical model using 3D-RBSM to evaluate crack propagation due to rebar corrosion, to investigate the effects of modeling in several corrosion conditions such as local corrosion and penetration of corrosion into cracks, and to clarify a cracking mechanism of single rebar specimens. The experiment on single rebar specimens was carried out to verify the applicability of the proposed model. The following summary and conclusions were derived from the study.

(1) The proposed three-phase material corrosion-expansion model is appropriate to simulate corrosion-induced expansion pressure since properties of corrosion products could be assumed directly in the model. The values of the thickness and linear elastic modulus of corrosion products were set to 1 mm and 500 MPa, respectively, in the model.
(2) The local corrosion model after concrete cracking should be considered in the analysis rather than the uniform corrosion model since it strongly influenced the internal crack patterns.
(3) The penetration of corrosion products into cracks should be considered in the corrosion induced cracking analysis because it quantitatively influenced the crack propagation. The penetration threshold value is a sensitive parameter in the model. Further experiments are needed to evaluate this parameter.
(4) The proposed analytical model using 3D-RBSM was able to simulate efficiently the local corrosion and the penetration of corrosion products into cracks since crack widths and crack volumes could be obtained directly during the analysis.
(5) When the rebar corroded, visible cracks initiated from the specimen surface and then propagated toward the rebar. After that, the lateral cracks initiated and propagated with an increase of the surface crack widths. This mechanism was confirmed by the experimental results and the analytical results.
(6) Surface deformation measurements were evaluated using a laser displacement meter. The mechanism relating surface deformation, surface crack propagation, and internal crack propagation was confirmed. That is, the surface deformation and the surface crack propagation were strongly dependent on the internal crack propagation. Therefore, in order to evaluate the surface crack propagation, the internal crack propagation should be precisely evaluated in the analysis.
(7) The results of the analytical model were verified qualitatively and quantitatively against the experimental results and they showed generally reasonable agreement, not only in the values but also in the propagation tendency. The proposed model would be a good reference for future development of analysis methods for concrete structures under corrosive environments.
(8) In the proposed model, the fictitious thickness (H) of the corrosion products layer is kept constant in the simulation, which is different from the real-world problem. In future study, we will take into consideration changing thickness of corrosion products layer during the analysis.

References

[1] Andrade C, Alonso C, Molina FJ. Cover cracking as a function of bar corrosion: Part I – Experimental test. Mater Struct 1993;26:453–64.
[2] Cabrera JG. Deterioration of concrete due to reinforcement steel corrosion. Cement Concr Compos 1996;18:47–59.
[3] Toongoenthong K, Maekawa K. Simulation of coupled corrosive product formation, migration into crack and propagation in reinforced sections. J Adv Concr Technol 2005;3(2):253–65.
[4] Val VD, Chernin L, Stewart GM. Experimental and numerical investigation of corrosion-induced cover cracking in reinforced concrete structures. J Struct Eng, ASCE 2009;135:376–85.
[5] Wang L, Soda M, Ueda T. Simulation of chloride diffusivity for cracked concrete based on RBSM and truss network model. J Adv Concr Technol 2008;6(1):143–55.
[6] Kawamura K, Nakamura H, Kunieda M, Ueda N. A fundamental study about the evaluation of crack propagation in concrete induced by rebar corrosion. In: Proceeding of JCI meeting, vol. CD. Japan Concrete Institute; 2009. p. 1075–80 [in Japanese].
[7] Tran KK, Kawamura K, Nakamura H, Kunieda M. Prediction of cracking of concrete due to rebar corrosion using 3D-RBSM. In: Proceedings of the eleventh international summer symposium, JSCE; 2009. p. 249–52.
[8] Oh BH, Kim KH, Jang BS. Critical corrosion amount to cause cracking of reinforced concrete structures. ACI Mater J V 2009;106(4):333–9.
[9] Nguyen QT, Millard A, Care S, L'Hostis V, Berthaud Y. Fracture of concrete caused by the reinforcement corrosion products. J Phys IV France 2006;136:109–20.
[10] Kawamura K, Tran KK, Nakamura H, Kunieda M. Surface crack propagation behavior against the surface deformation and inside cracks due to rebar corrosion. In: Proceeding of JCI meeting, vol. 32(1). Japan Concrete Institute; 2010, p. 1007–12 [in Japanese].
[11] Kawai T. New element models in discrete structural analysis. J Soc Naval Architects Japan 1977;141:187–93.
[12] Kawai T, Takeuchi N. Discrete limit analysis program, series of limit analysis by computer, vol. 2. Tokyo: Baifukan; 1990 [in Japanese].
[13] Bolander JE, Saito S. Fracture analysis using spring network models with random geometry. Eng Fract Mech 1998;61:569–91.
[14] Ueda M, Kei T, Taniguchi H. Discrete limit analysis of reinforced concrete structures by RBSM. Proc JCI 1988;10(3):335–8 [in Japanese].
[15] Nagai K, Sato Y, Ueda T. Mesoscopic simulation of failure of mortar and concrete by 2D RBSM. J Adv Concr Technol 2004;2(3):359–74.
[16] Yamamoto Y, Nakamura H, Kuroda I, Furuya N. Analysis of compression failure of concrete by three dimensional rigid body spring model. Doboku Gakkai Ronbunshuu 2008;64(4):612–30 [in Japanese].
[17] Saito S. Fracture analyses of structural concrete using spring network with random geometry. Doctoral thesis. Kyushu University; 1999.
[18] Lundgren K. Modeling the effect of corrosion on bond in reinforced concrete. Mag Concrete Res 2002;54(3):165–73.
[19] Matsuo T, Nishiuchi T, Matsumura T. Crack propagation analysis in concrete induced by rebar corrosion expansion. Concr J, Japan Concr Inst 1997;19:99–104 [in Japanese].